Exploring the Potential of Zinc Ferrite Nanocomposite as an Anode Material in Lithium-Ion Batteries: Integration with Fish Scale-Derived Carbon Support for Enhanced Performance

Suqqyana Fazal[1], Fawad Ahmad[1*], Khizar Hussain Shah[2], Shabnam Shahida[3], Tauqeer Ahmad[4], Gulfam Nasar[5*]

[1] Department of Chemistry, University of Wah, Quaid Avenue, Wah Cantt., (47010), Punjab, Pakistan
[2] Department of Chemistry, COMSATS University Islamabad, Islamabad Campus, Islamabad 45000, Pakistan
[3] Department of Chemistry, University of Poonch, Rawalakot, Azad Kashmir 12350, Pakistan
[4] Department of Chemistry, University of Mianwali, Mianwali 42200, Pakistan
[5] Department of Chemistry, Faculty of Basic Sciences, Balochistan University of Information Technology, Engineering and Management Sciences, Quetta (87100), Pakistan

ARTICLE INFO	ABSTRACT
	For lithium-ion batteries, excellent anode materials are recognized as ternary zinc-based oxides. Due to metal oxides' poor cycling stability, rapid capacity deterioration, and poor rate performance, their use as battery anodes reduces their applicability. However, by reducing the material's particle size and loading it on activated and non-activated carbon, the electrochemical performance gets improved. $ZnFe_2O_4$ is prepared hydrothermally and analyzed by an X-ray diffractometer to determine the $ZnFe_2O_4$ pure phase. SEM data shows that the particle's diameters ranged from 20 to 140 nm. Its 1015 mAh/g capacity after 100 cycles and maintenance cycle stability compared to other anode materials proves it's an excellent anodic material for lithium-ion batteries.

*Corresponding Authors' Email: fawad.ahmad@uow.edu.pk, gulfam.nasar@buitms.edu.pk

1. Introduction

Due to their extended cycle life and high energy density, lithium-ion batteries (also called LIB) are viewed as viable new power sources for portable electronic gadgets as well as for electric hybrid cars. The dendritic lithium development on the surface of the anode at high charging current would be one of the significant safety concerns in LIBs for hybrid electric vehicles since the traditional carbonous material approaches nearly zero V versus Li/Li^+ towards the conclusion of Li insertion (Cheng, Shapter, Li, & Gao, 2021). The lithium battery cannot function without the anode. The anode material currently has greater opportunities for advancement than the cathode material. Graphite, the primary anode material currently in use, has an inadequate specific capacity and cannot satisfy consumer demand for high-performance lithium batteries (Divakaran et al., 2021). Transition metal oxide electrodes, such as ZnO, MnO, Fe_2O_3, and NiO, have outstanding cycle performance, flexible operating voltage, and high theoretical specific capacities (500–1000 $mAhg^{-1}$) (Athika et al., 2019; Orisekeh et al., 2021). TMO anode materials provide better stability and specific capacity when compared to commercially available graphite anodes since they can prevent lithium dendrites (Zhang et al., 2021). It costs less to produce alloy anode materials than metals. However, numerous issues still need to be resolved, such as electrolyte decomposition (Tsai, Kuo, Liu, Lee, & Yew, 2021). Due to the synergistic properties of iron along with the other transition metal presence, spinel mixed transition metal oxides based on iron (MFe2O4, where M = Zn, Cu, Mn, Co, etc.) are being suggested as natural alternative anode materials for high-performance lithium-ion batteries (Trandafir et al., 2023; ul Ain, Fazal, & Ahmad, 2023). Zinc Ferrite (ZFO), in contrast to other oxides employed, has a lithium insertion process, including alloying and conversion events

(Appiah-Ntiamoah, Baye, & Kim, 2020). ZFO is very interesting because of its low cost, abundant supply of eco-friendly Zn and Fe elements, large surface-to-volume ratio, relatively short path for Li-ion diffusion, the low working voltage of about 1.5 V for lithium extraction, and, most importantly, high theoretical specific capacity (1072 mA h g-^{1}) (Jiang et al., 2018; Nivetha & Grace, 2019). However, $ZnFe_2O_4$ suffers from the same issue as other anode materials in that it is susceptible to significant volume expansion during the insertion and removal of lithium ions (Bini, Ambrosetti, & Spada, 2021; Spada et al., 2023). Volume change results in cracking, crushing, and even separating some active ingredients from the collector, which affects the battery's ability to cycle and charge quickly and how much capacity it can hold (Li et al., 2019). The iron-based anode material's particle size is decreased to the nanoscale level to alleviate this issue and provide stable battery operation. As a result, physical stress may be decreased, nanomaterials' lithium-ion battery reaction times can be sped up, the ion diffusion channel can be condensed, and the specific surface area can be raised to ensure that the electrode material makes complete contact with the electrolyte (Lv, Wang, Zhang, Shi, & Shi, 2022). Due to carbon's porous structure, its presence can offset some of the adverse effects of ZFO's volume alterations (Ghule, Shaikh, & Mane, 2020). As a result of their chemical composition, fish scales are one of the most promising carbon sources (Zingare, Dhoble, & Deshmukh, 2022). These are a cheap and convenient source of carbon-free biomass because of easily accessible.

In this research, fish scale-derived carbon (FSC) is added as an amorphous skeleton, and by using a hydrothermal process, the heterostructure of Zinc ferrite is anchored to the RHC matrix. One of them, a matrix of carbon made of biomass, is anticipated to reduce the volume that expands nanoparticles of oxide during charge and discharge while also enhancing the conductivity of the active material. A sample of zinc iron oxide is made without using the carbon nanocomposites method and then heated in an argon environment. Following that, measurements using cyclic voltammetry, LSV, EIS, and X-ray diffraction are made to connect the identified structural, morphological, and electrochemical features.

2.   Materials and Synthesis

Zinc nitrate hexahydrate, Iron nitrate hexahydrate, Hydrochloric Acid, Sodium Hydroxide. Ammonia water, Urea, Ethanol, and fish scales were used for the synthesis.

40 mmol Urea was dispersed into a solution of 100ml distilled water and 100ml ethanol. The solution was marked as Solution A, and Solution A was fully stirred. 4mmol Zinc nitrate hexahydrate and 4mmol Iron nitrate hexahydrate were dispersed in a solution of 50ml distilled water and 50ml ethanol. The solution was stirred for 30 minutes and named Solution B. Solution B was slowly dripped into Solution A, then 15ml of ammonia water and 20ml distilled water were added to it. The mixed solution was stirred for half an hour. After stirring for half an hour, the solution was transferred to a 500 ml china dish, maintained at 130 °C for 12 h. The obtained solution was washed three times with distilled water and ethanol until neutrality was achieved.

2.1.   Preparation of Activated Carbon

Labeo rohita (rohu) fish scales were taken from the market. Tap water was used for washing, and hot and cold distilled water was used to remove dirt and impurities. Then, they were shelter dried thoroughly for three days. Using a mixer grinder, they were broken into tiny pieces. The percentage of crushed material that passed through a 600 m sieve but was kept on a 125 m screen was collected. It was then converted to charcoal in a muffle furnace at 600ºC. This material was then chemically activated by acid/base treatment. Acid activation was performed using 10g of fish scale powder combined with 150 ml 0.1M HCl solution for 2.5 hours at room temperature on a 100rpm heating plate. Base activation was also performed as same using 0.1M NaOH. It was then vacuum filtered, obtained semi-slurry, and rinsed with distilled water until it reached pH=7. After that, the sample was oven-dried at 60º Celsius. The prepared activated carbon material was cooled and stored in a desiccator.

2.2. Preparation of ZnFe₂O₄/AC

Zinc ferrite nanocomposite and Activated carbon from fish scales were combined in a 3:7 ratio, dissolved in 30 mL of distilled water, and agitated for 30 minutes. The prepared sample was moved into a 50 mL china dish and treated there for 24 hours at 200 °C before being twice washed using ethanol and distilled water. The dried prepared material was placed at 60 °C in the oven. This item was identified as $ZnFe_2O_4$/AC.

2.3. Preparation of ZnFe₂O₄/NAC

Zinc ferrite nanocomposite and non-activated carbon from fish scales were combined in a 3:7 ratio, dissolved in 30 mL of distilled water, and agitated for 30 minutes. The prepared sample was moved into a 50 mL china dish and treated there for 24 hours at 200 °C before being twice washed using ethanol and distilled water. The dried prepared material was placed at 60 °C in the oven. This item was identified as $ZnFe_2O_4$/NAC.

3. Results and Discussion
3.1. XRD Analysis

The XRD method was used to conduct a crystallographic examination of the synthesized material. The XRD graphs for the Zinc ferrite nanocomposites and ZFO/C samples are shown in the figure. The absence of specular diffractions denotes crystallographic purity (Kiruthika, Lakshmi, Diana, Helen, & Selvin, 2022). It confirmed that the synthesized substance is pure because no impurity peaks were seen. The XRD peaks corroborated the formation of ZFO (220), (311), (400), (422), (333), (440), at 30.01, 35.43,42.98, 53.21 56.81, and 62.16 described in the literature as shown in FIG 1(a) (Parvathi & Ramesan, 2023). The data determined the crystallite size to be 22.49 nm. The intense diffraction peaks are the key evidence for the current sample's excellent crystallinity.
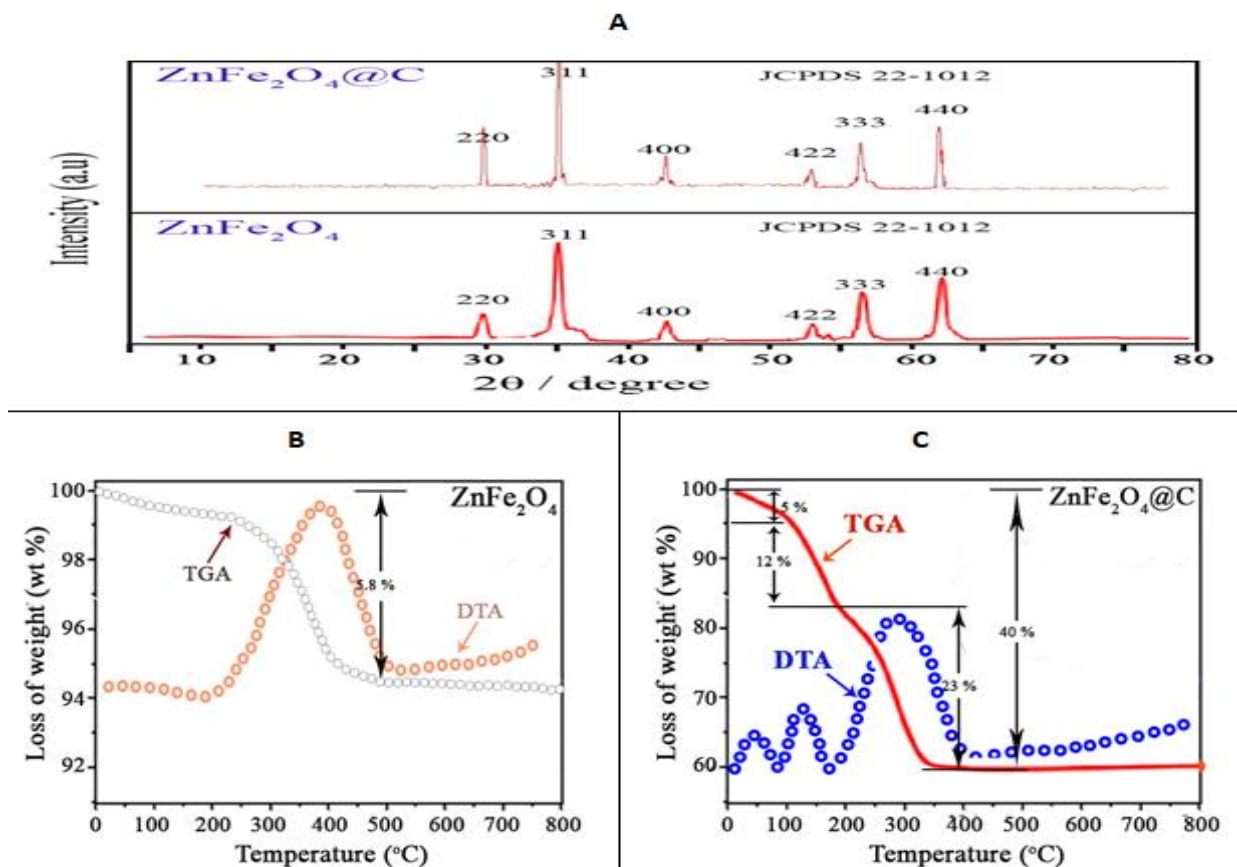
Figure 1: (a) XRD of ZFO and ZFO/AC (b) TGA of ZFO (c) TGA of ZFO/AC

Furthermore, all the peaks appearing in the XRD pattern are attributed to zinc iron oxide. No additional intermediate states, such as ZnO and Fe_2O_3, are detected, indicating

3

the complete chemical reaction. An expert high score has been used, and the position and relative strength of the diffraction peaks agree well with the conventional Zinc Iron oxide diffraction data (JCPDS22- 1012), as shown in the image. The formation of the ZFO/C nanocomposite is made apparent by sharp peaks given by the sample ZFO/C than by pure zinc ferrite nanocomposite (Baynosa et al., 2020).

According to ZFO's TGA data, zinc ferrite degrades in a single step between 200 and 500°C, losing 5.8% of its zinc content as coordinated metal connections break (Karthikeyan, Sirajudheen, Nikitha, & Meenakshi, 2020). On the other hand, ZFO/C degrades in three steps and becomes steady above 320°C.

3.2. SEM Analysis

High-resolution SEM examination was used to evaluate the surface shape and grain size of the synthesized ZFO/C nanocomposite. The granules in the figure are evenly dispersed shown in FIG 2(c). Agglomeration might arise as a result of magnetic interaction between nanoparticles. Aggregation of smaller grains is also conceivable, giving birth to grain boundary regions that may be seen distinctly at the outer edges of some of the grains. The maximum and minimum particle sizes calculated through nano measure are 141.56nm and 15.69nm under a 500nm scanning lens. The average number of particles present is 76.18nm. The maximum and minimum particle sizes calculated through nano measure are 0.34um and 0.07um under a 1um scanning lens. The average number of particles present is 0.19um. The average particle shape is irregular, but the size is uniform, as shown in FIG 2(a).
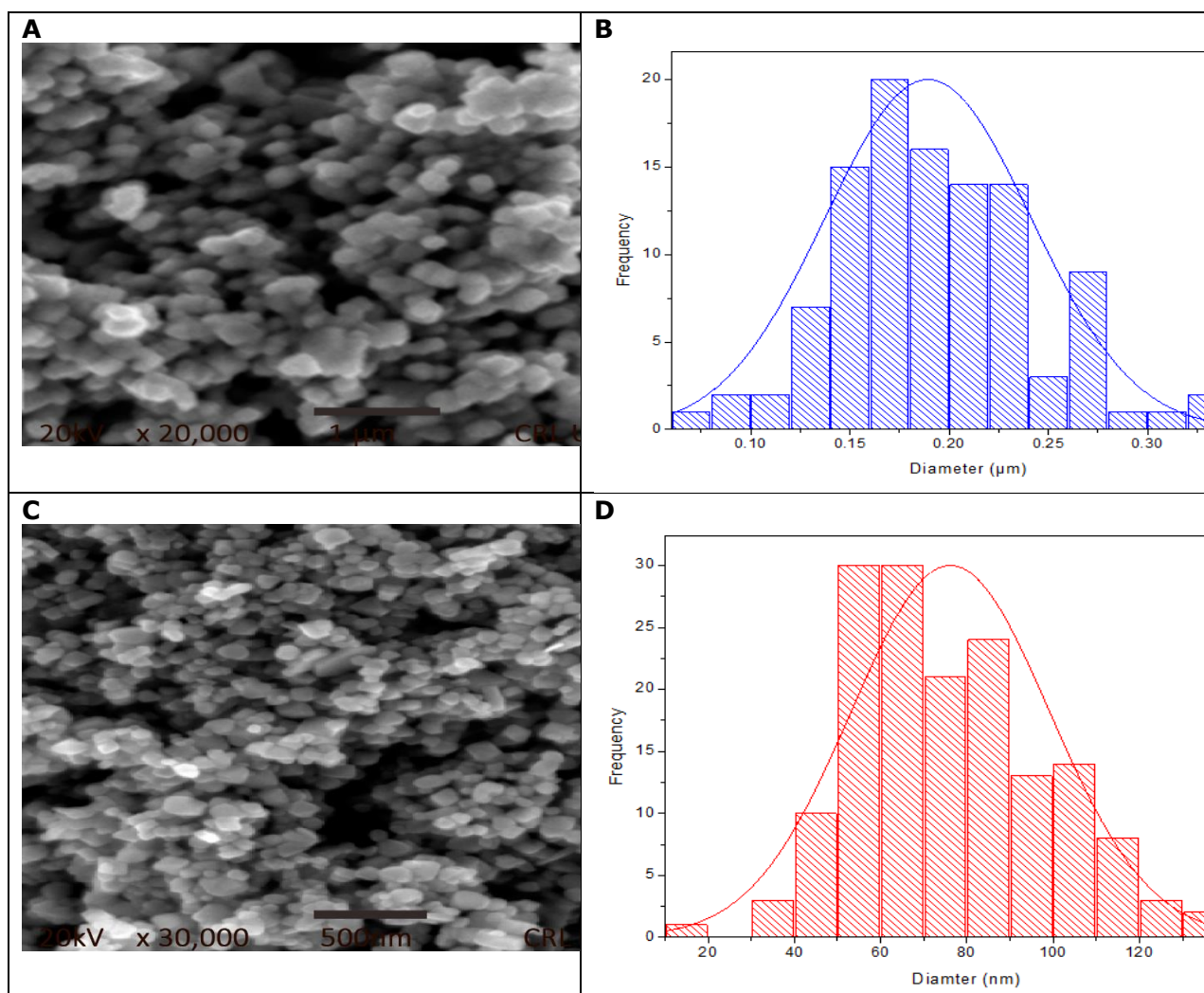
Figure 2: (a)(b) SEM and distribution plot at 1μm scanning lens (c)(d) SEM and distribution plot at 500nm scanning lens

3.3. Electrochemical Studies

To evaluate the electrochemical characteristics of zinc ferrite nanocomposite and its sample with non-activated carbon support and activated carbon support, each sample was independently coated on the glassy carbon electrode (working electrode). The broad minor tumid at about 1.1 V creates a solid-electrolyte interface (SEI) as an outcome of the electrolyte decomposition.
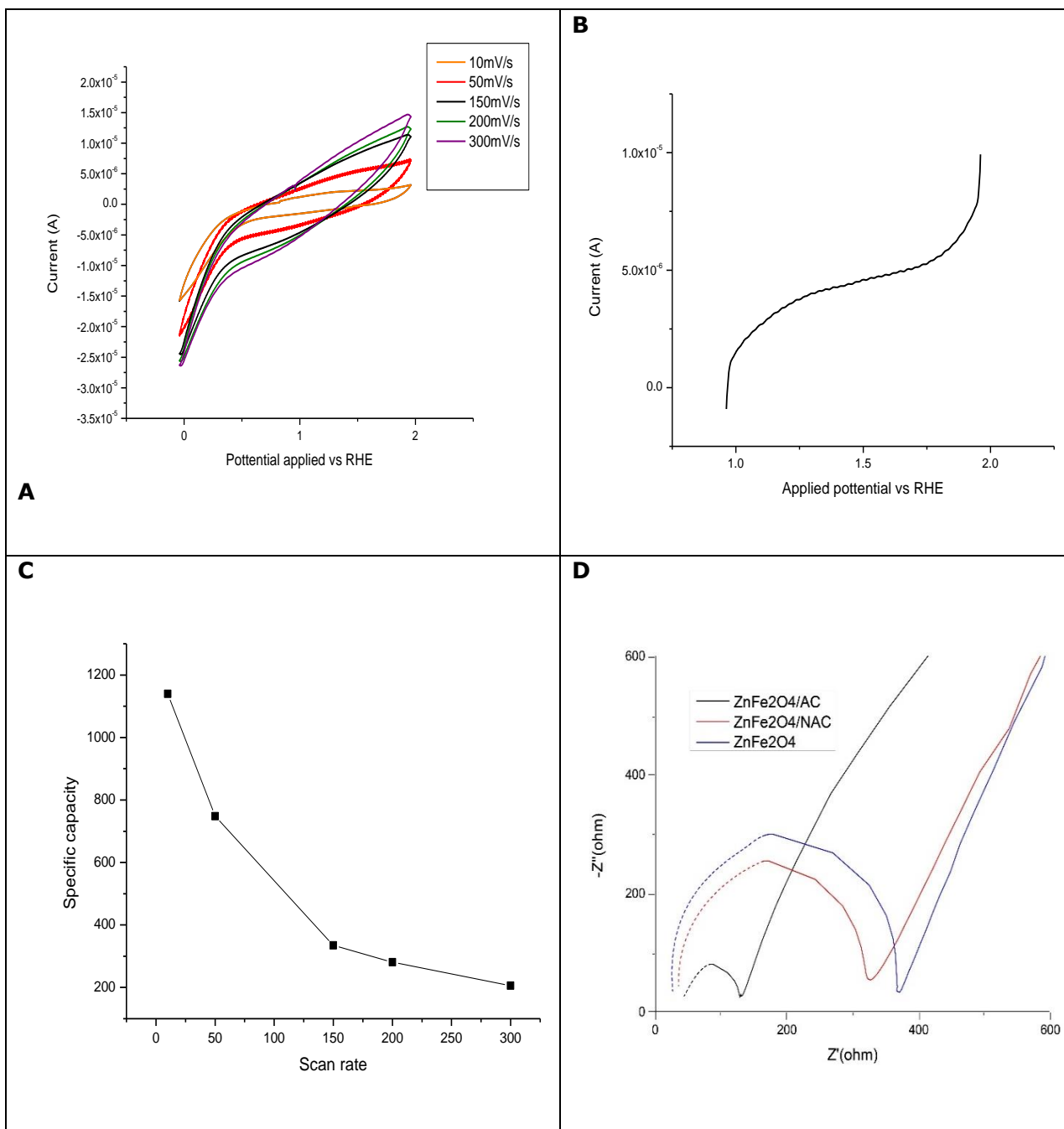
Figure 3: (a) CV of ZFO (B) LSV of ZFO (c) SR Vs. Specific capacity (d) EIS of ZFO, ZFO/NAC, and ZFO/AC

The most pronounced strong reduction peak at 0.9 V is caused by the irreversible reduction of Zn^{2+} and Fe^{3+} from the $Li_xZnFe_2O_4$ crystals to metal Zn and Fe and the alloying process of Zn to LiZn. The anodic curves, however, continue to have the same general shape. As there is no loss of Li^+ from the LiZn alloy, no mild oxidation peak is shown between 0.14 and 0.26 V (Xu et al., 2021). The noticeable oxidation peak is then found at 1.20-1.98 V, caused by the reversible conversion of Zn and Fe metals to ZnO and Fe_2O_3 (Wei et al., 2019). An outline of all potential anode reactions from equations (1-5).

5

$$ZnFe_2O_4 + xLi^+ + xe^- \rightarrow Li_xZnFe_2O_4 \tag{1}$$
$$Li_xZnFe_2O_4 + (nx)Li^+ + (nx)e^- \rightarrow Zn + 2Fe + 4Li_2O \tag{2}$$
$$Zn + Li^+ + e^- \leftrightarrow LiZn \tag{3}$$
$$ZnO + 2Li^+ + 2e^- \leftrightarrow Zn + Li_2O \tag{4}$$
$$Fe_2O_3 + 6Li^+ + 6e^- \leftrightarrow 2Fe + 3Li_2O \tag{5}$$
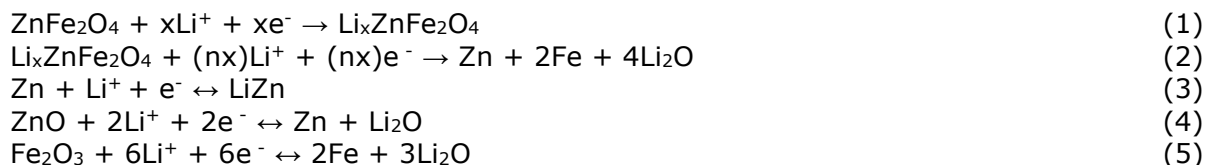
From LSV, 0.98V was determined as the onset potential FIG 2(b). The electrochemical events of reduction, oxidation, lithiation, delithiation, and SEI production for ZFO/C are identical to those in zinc ferrite nanocomposite (Bao et al., 2021). The greater surface area of CV in FIG 4(a)(b) demonstrates the difference in improved electrocatalytic activity attributed to the existence of porous carbon (Lee, Ahn, & Lee, 2022).
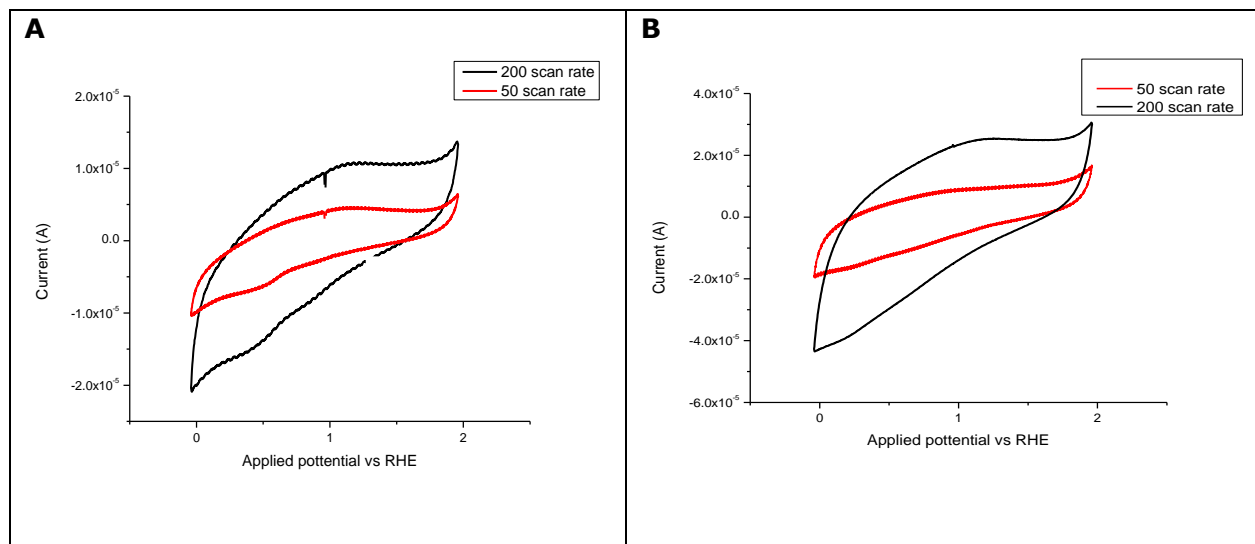
Figure 4: (a) CV of ZFO/NAC (b) CV of ZFO/AC

The calculated values of specific capacity given above show that due to the greater surface activity of Activated carbon ZFO/AC has the highest specific capacity (He, Wang, Tang, Zhang, & Wang, 2022). Greater charge storing capacity tends to have greater columbic efficiency of ZFO/AC (Liu et al., 2022).

Table 1
Specific capacity at 50mV/s, Current density, ECSA, and Columbic efficiency of prepared materials

Material	Specific capacity at 50mV/s	Current density (μAcm^{-2})	ECSA	Columbic efficiency
Zinc ferrite	748.8mAh/g	398.69	3.14E-02	74%
Zinc ferrite/NAC	882mAh/g	296.09	3.32E-02	89%
Zinc ferrite/AC	1115.6mAh/g	619.84	7.70E-02	98%

EIS was used to verify the developed material's conductivity further. Figure 2(d) displays the Nyquist plots as obtained, which are divided into linear and several semicircle sections. The inclined straight line is in the low-frequency band, while the semicircular region belongs in the higher frequency range. The intersection point, which is present at higher frequencies, provides information about "Rs," which stands for the material resistance that electrodes have by nature and the conflict that results from the contact of the working electrode with the collector. Diffusion resistance is provided by the straight line in the second section of the Nyquist plot. Of the linear line's more vertical nature, this resistance decreases (Zhao et al., 2022). Compared with ZFO/NAC and ZFO/AC materials, bare ZFO has displayed a larger semicircle, suggesting that it offers strong solution resistance. Rise in the fictional portion of the plot demonstrated that the produced material performed well in terms of conductivity. The rise in the fictitious portion of the curve is more pronounced for ZFO/AC nanocomposite, showing that the electrode's material is more conducting than electrodes built of ZFO and ZFO/NAC.

After the first ten cycles, there is a noticeable decline in specific capacity and colombic efficiency, but stability is maintained for the following 100 cycles shown in FIG 5.
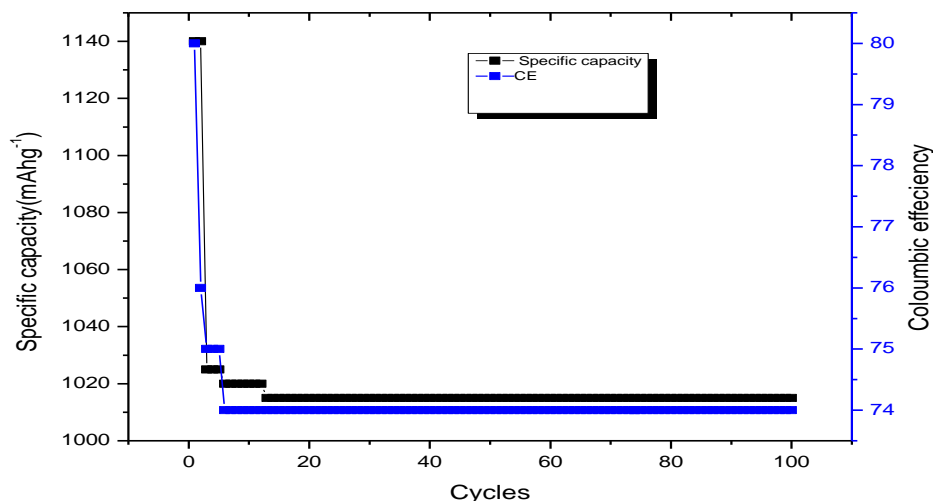
Figure 5: Cyclability of ZFO

Conclusion

The hydrothermal synthesis approach was used to create the $ZnFe_2O_4$ nanocomposites, which were also supported by carbon from fish scales. The current investigation results are completely coordinated with the standard chemically routed $ZnFe_2O_4/C$ samples. The XRD results show a crystalline structure with no traces of impurities, and the crystallite size is 23 nm. The uneven grain sizes of the morphological patterns range from 30 to 40 nm. Electrochemical testing demonstrates that ZFO/C exhibits higher specific capacity and activity on the surface than ZFO with no carbon support due to porous carbon support. It is noteworthy that $ZnFe_2O_4$ nanoparticles exhibit well-stable cycle performance in addition to high reversible capacity. In a nutshell, ZnFe2O4/C nanocomposite is appropriate as an anode material for use in various future scenarios.

Reference

Appiah-Ntiamoah, R., Baye, A. F., & Kim, H. (2020). In Situ Electrochemical Formation of a Core-Shell ZnFe2O4@ Zn (Fe) OOH Heterostructural Catalyst for Efficient Water Oxidation in Alkaline Medium. *ChemElectroChem, 7*(16), 3478-3486.

Athika, M., Prasath, A., Sharma, A. S., Devi, V. S., Duraisamy, E., & Elumalai, P. (2019). Ni/NiFe2O4@ carbon nanocomposite involving synergistic effect for high-energy density and high-power density supercapattery. *Materials Research Express, 6*(9), 095503.

Bao, S., Tan, Q., Kong, X., Wang, C., Chen, Y., Wang, C., & Xu, B. (2021). Engineering zinc ferrite nanoparticles in a hierarchical graphene and carbon nanotube framework for improved lithium-ion storage. *Journal of colloid and interface science, 588*, 346-356.

Baynosa, M. L., Mady, A. H., Kumar, D. R., Sayed, M. S., Tuma, D., & Shim, J.-J. (2020). Eco-friendly synthesis of recyclable mesoporous zinc ferrite@ reduced graphene oxide nanocomposite for efficient photocatalytic dye degradation under solar radiation. *Journal of colloid and interface science, 561*, 459-469.

Bini, M., Ambrosetti, M., & Spada, D. (2021). ZnFe2O4, a green and high-capacity anode material for lithium-ion batteries: A review. *Applied Sciences, 11*(24), 11713.

Cheng, H., Shapter, J. G., Li, Y., & Gao, G. (2021). Recent progress of advanced anode materials of lithium-ion batteries. *Journal of Energy Chemistry, 57*, 451-468.

Divakaran, A. M., Minakshi, M., Bahri, P. A., Paul, S., Kumari, P., Divakaran, A. M., & Manjunatha, K. N. (2021). Rational design on materials for developing next generation lithium-ion secondary battery. *Progress in Solid State Chemistry, 62*, 100298.

Ghule, B. G., Shaikh, Z. P., & Mane, R. S. (2020). Ferrites for batteries. In *Spinel Ferrite Nanostructures for Energy Storage Devices* (pp. 147-172): Elsevier.

He, X., Wang, X., Tang, M., Zhang, H., & Wang, Y. (2022). Self-supporting ZnP2@ N, P co-doped carbon nanofibers as high-performance anode material for lithium-ion batteries. *Journal of Alloys and Compounds, 897*, 163235.

Jiang, L., Gao, W., Jin, B., Li, H., Li, S., Zhu, G., & Jiang, Q. (2018). ZnFe2O4/MoS2/rGO composite as an anode for rechargeable Lithium-ion batteries. *Journal of Electroanalytical Chemistry, 823*, 407-415.

Karthikeyan, P., Sirajudheen, P., Nikitha, M. R., & Meenakshi, S. (2020). Removal of phosphate and nitrate via a zinc ferrite@ activated carbon hybrid composite under batch experiments: study of isotherm and kinetic equilibriums. *Environmental Nanotechnology, Monitoring & Management, 14*, 100378.

Kiruthika, T., Lakshmi, D., Diana, M. I., Helen, P. A., & Selvin, P. C. (2022). One-step green synthesis of ZnFe2O4 anodes for Li-ion batteries. *Materials Today: Proceedings, 68*, 2753-2758.

Lee, D. K., Ahn, C. W., & Lee, J. W. (2022). TiO2/Carbon Nanosheets Derived from Delaminated Ti3C2-MXenes as an Ultralong-Lifespan Anode Material in Lithium-Ion Batteries. *Advanced Materials Interfaces, 9*(10), 2102375.

Li, Y., Meng, Y., Liu, X., Xiao, M., Hu, Q., Li, R., . . . Zhu, F. (2019). Double-protected zinc ferrite nanospheres as high rate and stable anode materials for lithium ion batteries. *Journal of Power Sources, 442*, 227256.

Liu, X., Zhu, S., Liang, Y., Li, Z., Wu, S., Luo, S., . . . Cui, Z. (2022). 3D N-doped mesoporous carbon/SnO2 with polypyrrole coating layer as high-performance anode material for Li-ion batteries. *Journal of Alloys and Compounds, 892*, 162083.

Lv, X.-N., Wang, P.-F., Zhang, Y.-H., Shi, Q., & Shi, F.-N. (2022). MOF-derived CoFe2O4/FeO/Fe nanocomposites as anode materials for high-performance lithium-ion batteries. *Journal of Alloys and Compounds, 923*, 166316.

Nivetha, R., & Grace, A. N. (2019). Manganese and zinc ferrite based graphene nanocomposites for electrochemical hydrogen evolution reaction. *Journal of Alloys and Compounds, 796*, 185-195.

Orisekeh, K., Singh, B., Olanrewaju, Y., Kigozi, M., Ihekweme, G., Umar, S., . . . Soboyejo, W. (2021). Processing of α-Fe2O3 nanoparticles on activated carbon cloth as binder-free electrode material for supercapacitor energy storage. *Journal of Energy Storage, 33*, 102042.

Parvathi, K., & Ramesan, M. (2023). High performance chlorinated natural rubber/zinc ferrite nanocomposite prepared through industrial compounding technique. *Polymer Bulletin, 80*(3), 3165-3182.

Spada, D., Ambrosetti, M., Mozzati, M. C., Albini, B., Galinetto, P., Cini, A., . . . Bini, M. (2023). Understanding the electrochemical features of ZnFe2O4, anode for LIBs, by deepening its physico-chemical properties. *Materials Research Bulletin, 160*, 112132.

Trandafir, E. V., Trassinelli, M., Prigent, C., Steydly, S., Vernhet, D., & Caltun, O. F. (2023). Ferrite nanoparticles and thin films irradiated by slow highly charged ion beams. In *Ferrite Nanostructured Magnetic Materials* (pp. 391-405): Elsevier.

Tsai, Y.-C., Kuo, C.-T., Liu, S.-F., Lee, Y.-T., & Yew, T.-R. (2021). Effect of different electrolytes on MnO2 anodes in lithium-ion batteries. *The Journal of Physical Chemistry C, 125*(2), 1221-1233.

ul Ain, Q., Fazal, S., & Ahmad, F. (2023). Synthesis of bimetallic iron ferrite and its applications in alcohol fuel cell. *Journal of Chemistry and Environment*, 1-13.

Wei, D., Xu, F., Xu, J., Fang, J., Wang, G., Koh, S. W., & Sun, Z. (2019). A critical electrochemical performance descriptor of ferrites as anode materials for Li-ion batteries: inversion degree. *Ceramics International, 45*(18), 24538-24544.

Xu, B., Yu, L., Zhao, X., Wang, H., Wang, C., Zhang, L. Y., & Wu, G. (2021). Simple and effective synthesis of zinc ferrite nanoparticle immobilized by reduced graphene oxide as anode for lithium-ion batteries. *Journal of colloid and interface science, 584*, 827-837.

Zhang, Y., Xie, M., He, Y., Zhang, Y., Liu, L., Hao, T., . . . Liu, N. (2021). Hybrid NiO/Co3O4 nanoflowers as high-performance anode materials for lithium-ion batteries. *Chemical Engineering Journal, 420*, 130469.

Zhao, Q., Peng, P., Zhu, P., Yang, G., Sun, X., Ding, R., . . . Liu, E. (2022). F-doped zinc ferrite as high-performance anode materials for lithium-ion batteries. *New Journal of Chemistry, 46*(20), 9612-9617.

Zingare, P. A., Dhoble, S. J., & Deshmukh, A. D. (2022). Highly stable fish-scale derived lamellar carbon for high performance supercapacitor application. *Diamond and Related Materials, 124*, 108925.